

A three-dimensional finite element foot-ankle model and its personalisation methods analysis

Fuhao Mo ^{a,*}, Yuandong Li ^a, Junjie Li ^a, Shuangyuan Zhou ^{b,*}, Zurong Yang ^c

^a State Key Laboratory of Advanced Design and Manufacture for Vehicle Body, Hunan University, Changsha, Hunan 410082, China

^b Department of Radiology, Xiangya Hospital, Central South University, Changsha, Hunan 410011, China

^c Department of Ultrasound Diagnosis, Second Xiangya Hospital of Central South University, Changsha, Hunan 410008, China

ARTICLE INFO

Keywords:

Biomechanics
Foot
Ankle
Gait
Personalisation
Finite element modeling

ABSTRACT

Foot and ankle injuries are common as a result of overuse or trauma as well as various pathologies. This study aims to establish a three-dimensional foot-ankle model and investigate its suitability personalisation for the analysis of foot-ankle biomechanical responses during dynamic gait loading. The model was first established based on medical images and validated in both static standing posture and dynamic gait loading concerning regional plantar pressures and the centre of pressure curve (COP). Then, two model personalisation methods using magnetic resonance imaging (MRI) and fast optical scan data, respectively, were investigated and compared through analysing the dynamic gait responses of the scaled models. In both methods, material personalisation of plantar tissues was also combined through supersonic shear wave elastography (SWE) measurements. With regard to plantar pressure distribution and internal soft tissue strain, both personalisation methods correlated well with the subject-specific experimental results. Thus, we believe that the present model, with a fast optical scan personalisation method of specific SWE measurement, is a reasonable arrangement for subject-specific plantar deformation behaviour analysis during dynamic gait loading.

1. Introduction

Although not life-threatening, foot and ankle injuries are frequent owing to overuse, trauma, and other ailments. The foot and ankle sustain complicated and high loads to support the body during locomotion and other activities as well as suffer various pathologies [1]. Biomechanical assessment on the foot and ankle region is essential for injury mechanism analysis, prosthetic design, surgery prediction, and so on. Potential experimental methods of foot and ankle biomechanics can provide a general overview; however, internal tissue responses, like stress and strain distribution, are difficult to measure *in vivo*. By calculating the deformation behaviour of internal tissues using the finite element (FE) model, complementary tools and new pathways can be developed to understand the mechanisms of various injuries and further apply novel treatment strategies and optimizations to clinically relevant scenarios [2].

Several FE foot-ankle models have been developed to overcome the experimental limitations of clinical-related applications [3–7], which have proved to be highly useful in understanding foot-ankle biomechanics and foot-ankle-related pathologies. However, the complex

geometry and nonlinear mechanical behaviour of foot tissue render any analytical solution practically impossible without simplifications in terms of morphology and function [4]. These simplifications can potentially impair the prediction of internal tissue stress and strain, plantar pressure, and joint kinematics, and limit their practical application [4,8,9]. According to previous studies [4,10,11], existing FE models have several limitations at both developmental and validation levels. Many previous models were validated with specific experimental results concerning their application fields; however, their applicability was limited owing to the time of publication. As experimental data are continuously obtained, new information is available for the establishment and validation of models [12–16]. Most previous models typically used quasi-static gait phases to represent realistic dynamic gait validation [4,10,17]. A few recent studies achieved continuous gait loading simulation [1,9,18–20].

In addition, one of the main challenges for the implementation of FE modelling in clinical practice is the development of reliable and affordable techniques for the subject-specific modelling of the foot [21,22]. However, constructing FE models based on medical images is time-consuming. Many previous studies used a general and single foot

* Corresponding author.

E-mail addresses: fuhao@hnu.edu.cn (F. Mo), zsy_amory1003@163.com (S. Zhou).

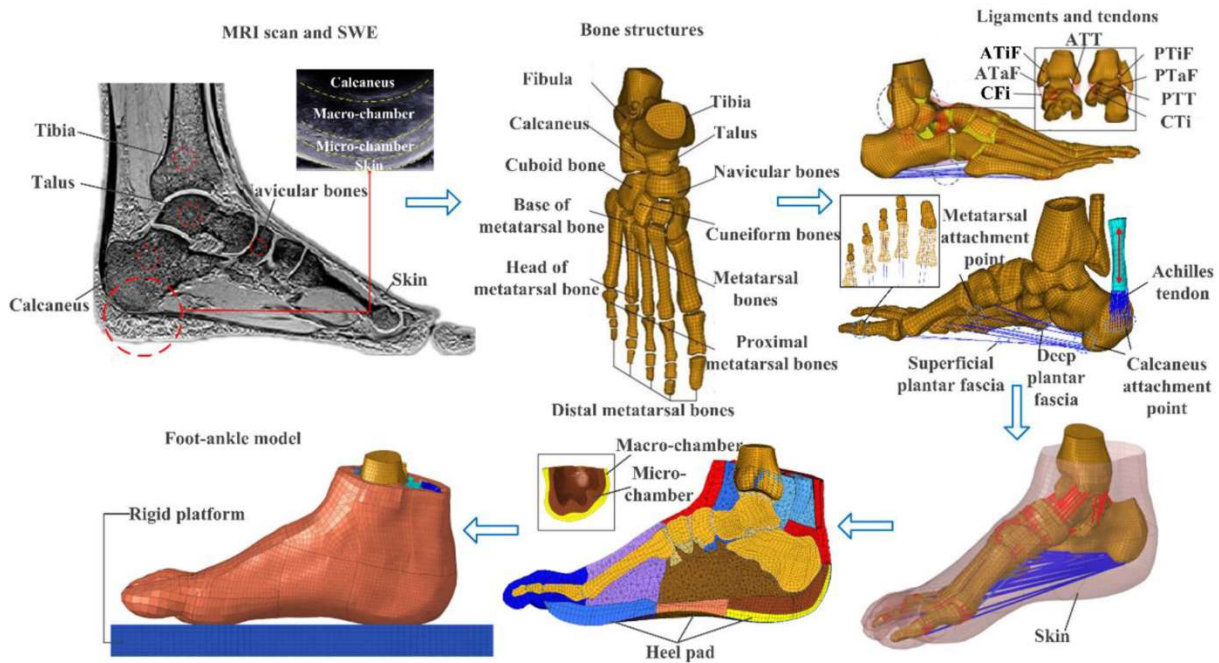


Fig 1. Overview of a finite element foot-ankle model setup from medical scans to bone structure, filled soft tissues and detailed connections.

FE model [3,5,7,9,23]. A few discussed individual modelling methods for clinical application [24,25]. Others [26–28] established statistical shape models (SSM) to be scaled for a later personalised design. On the other hand, some studies established a subject-specific model [29,30] and scaled it differently. Most of these studies are more focused on the geometric difference between the scaled and the original models. For an

FE model, the difference in simulation results can be more crucial for subsequent analysis.

Thus, this study intends to globally validate a three-dimensional foot-ankle finite element model by reviewing a series of gait experimental data and explore its personalisation methods through the comparative analysis of their dynamic gait simulation results. A subject-

Table 1
Summary of model materials and element types

Component	Element type	Material types	Density(g/mm ³)	Young modulus(MPa)	Stiffness N/mm	Poisson's ratio	Thickness (mm)	Reference
Tibia & fibula	Hexahedral	Elastic-plastic	0.0016	1200	-	0.3	-	Mo et al. 2012 [36]
Foot cortical bones	Shell	Elastic-plastic	0.0018-0.002	12000-20000	-	0.3	1.5	Schuster et al. 2000 [41]
Foot trabecular bones	Hexahedral	Elastic-plastic	0.0016	7200	-	0.3	-	Nakamura et al. 1981 [42]
Cartilage	Hexahedral	Mooney-Rivlin	0.0018	45	-	0.4	-	Dakin et al. 2001 [43]
Skin	2D-Shell	Elastic	9.2e-4	1.17e-3	-	0.4	1.2	Al-Dirini et al. 2016 [41]
Ligaments	1D tension-only beam	Nonlinear	-	-	-	0.4	-	Funk et al., 2000 [44]; Shin et al., 2012 ^a Davis et al., 1996 [45]; Kura et al., 2001 [46]
Plantar fascia	1D tension-only beam	Nonlinear	0.001	-	203 N/mm (Resting length)	-	-	Kitaoka et al., 1994 [47]
Lateral Plantar fascia	1D tension-only beam	Nonlinear	0.001	-	166±35N/mm	-	-	Isvilanonda et al., 2015 [48]
Achilles tendon	1D tension-only beam	Nonlinear	-	a	201.8 N/mm 0.209 mm	-	-	Morrison et al., 2015 [49]
Other tendons	1D tension-only beam	Nonlinear	-	b	-	-	-	Maganaris et al., 1999 [50]; Magnusson et al., 2008 [51]; Zajac et al., 1989. [52]
Filled muscle	Tetrahedral	Ogden-QLV	0.00112	0.00952	-	0.495	-	Mo et al., 2020 [16]; Mo et al., 2019 [40].
Micro & Macro chambers	Hexahedral	Ogden	0.001	0.0612-0.0303	-	0.499	-	Mo et al., 2019 [34]; Erdemir et al., 2006 [53]

Notes: a. The resting length of the Achilles tendon was set to 0.209mm, and the stiffness was set as 201.8N/mm according to Morrison et al. (2015).

b. Force-strain curve for tibialis anterior tendon was extracted from Maganaris and Paul⁵⁰. That for gastrocnemius tendon was extracted from Magnusson et al. (2008). Other tendon force-strain curves were scaled from the tibialis anterior stress-strain curve based on tendon length, cross-section area, and 1.2 GPa Young's modulus⁵².

c. Non-linear ligament and tendon modeling method based on the previous studies (Nie et al, 2017a, 2017b) were adopted in the present model. The stiffnesses for the fascia and tendon are the slopes of linear parts of the nonlinear curves.

Table 2

Validation matrix of the model in both static and dynamic loading

Loading types	Items	References	Validation indexes
Quasi-static standing posture	Plantar compression	Cheung et al., 2006 [5]	Force-deformation curves
	Bone structure alignments	Bandholm et al., 2004 [56]; Cavanagh et al., 1997 [57]; Williams et al., 2000 [58]	Bone heights and angles in stance phase
Dynamic gait	Plantar pressure	Birtane et al., 2004 [59]; Cavanagh et al., 1987 [60]	Regional pressure and contact area corridors
	Plantar pressure	Bryant et al., 2000 [61]; Maetzler et al., 2010 [12]; Putti et al., 2007 [13]; Current experiments	Regional pressure and contact area corridors
	Center of Pressure	Buldt et al., 2018 [14]; Chiu et al., 2013 [15]	COP corridor

specific foot-ankle model was improved and fully validated from compression, static standing posture to dynamic gait loading, from regional pressure distribution to gait pressure variation and centre of pressure (COP) curve. Then, the simulation results of two personalisation methods based on magnetic resonance imaging (MRI) and optical scan data, respectively, were compared and analysed. In future, the model and its personalisation method will likely be used in various related clinical research fields.

2. Methods and materials

2.1. Model establishment

The establishment process of a foot-ankle model was first introduced in terms of its geometry, mesh selection, material, and element type settings. The geometry of the foot-ankle model was reconstructed based on medical images from a volunteer close to a 50th percentile Chinese male (173.1 cm height and 69.7 kg weight). Both ultra-low-dose computed tomography (ULD-CT) and MRI scans were used to obtain anatomical foot and ankle structures. All procedures were reviewed and approved by the ethics committee of Xiangya Second Hospital. The ethical review number is [clinical research] No. (2021-019).

All MRI scans were performed using a 3.0 T Magnetom Prisma MRI system (Siemens Ltd, Germany) at the Department of Radiology of Xiangya Hospital. Two scan solutions were conducted. The first was used for most soft tissues (pixel spacing 0.586 mm, voxel depth 0.6 mm, slice spacing 0.6 mm, slice thickness 0.6 mm, and the scan option was set to proton density water (PDW)). The second was for cartilage (sagittal interval at 0.5 and 0.9 mm intervals in both, the axial and coronal plane), and the scan options were PDW, fat saturation (FS), turbo spin echo (TSE). Sequent, medical engineering software Mimics (Materialise, version 21.0) and Geomagic Studio (Geomagic, version 12.0) were used to extract detailed anatomic structures and export them in stereolithography (.stl) file format. LS-Dyna codes (Livermore Software, Livermore, USA) were adopted as the model explicit dynamic solver by defining boundary conditions, component properties, and materials.

The modelling details of the present model are shown in Fig. 1. A total of 183076 elements was included. Bone tissues were modelled with combined solid and shell elements. Uniform cortical bone thicknesses based on the measurements and estimation of the CT images were used for the bones of the foot. The inner regions were filled with trabecular

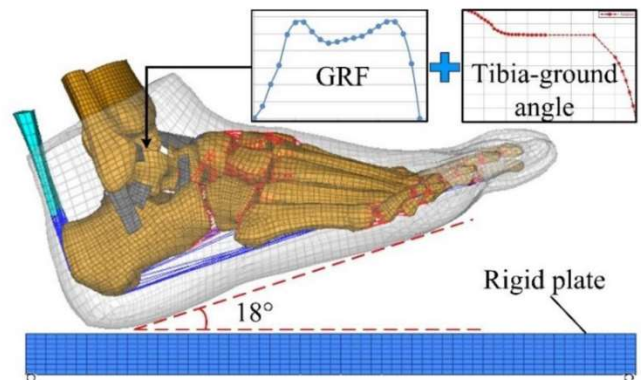


Fig 2. Validation setting of dynamic gait simulation. Imposing a rotation angle-time series at the talus and a normalized ground reaction force (GRF)-time series under foot based on the experimental data to simulate realistic gait loading condition of a human foot-ankle segment.

bones. Totally, 12 nonlinear and tension-only beams were defined to simulate middle and lateral plantar fascia by connecting insertion nodes on the bones. The biofidelity of the model was enhanced by segmenting the heel pad into three layers based on anatomical structure: macro-chamber, micro-chamber, and dermis [31–33], as reported in our previous paper [34].

Model material selections and element types are listed in Table 1. Bone tissues were modelled with an elastoplastic material model of Cowper and Symonds law. Strain rates coefficients of C and P are assigned as 360.5 and 3.6, respectively, based on literature analysis [35], which was also used in our previous models [36,37]. Ligaments, tendons, and plantar fascia were modelled with 1D tension-only beam and spring elements, while force-deformation curves were defined according to the previous literature [6,38,39]. The heel pad and filled muscles of the model were governed by a hyperelastic model of the first-order Ogden law, as reported and recommended in previous studies [34,37,40].

2.2. Deformation and kinematics evaluation of the foot-ankle FE model

Table 2 summarises the model validation matrix used to globally evaluate biomechanical responses of the present foot-ankle model, including both static standing posture and dynamic gait loading condition. Based on the review of previous experimental results [8,34,54,55] and new implemented gait experiments, both internal tissue deformation and pressure responses were evaluated through the model. The details about the validation process are introduced in the following sections.

Human static standing postures vary from individual to individual, depending on the foot type (planus, normal, or cavus). Potential foot pathologies can be also noted in this manner. Three types of experiments from the previous literature were employed to gradually improve and validate the model robustness in static standing. The detailed validation process and results obtained under static loading have been reported in our previous study [34]. Here, a summary is presented.

First, the plantar compression experiments of Cheung et al. were selected considering their simple loading conditions and a proper corridor of force-deformation curves [5]. Defining the plantar tissue properties was essential for the validation of this experiment. According to the experimental test conditions, the foot-ankle model was fixed at the cross-section above the ankle joint, and an axial load up to 700 N was exerted on a plate under the foot model. No Achilles tendon force was applied. Second, the foot bone structure alignments were compared with the previous studies [56–58] considering a quiet stance. Finally, plantar pressure data from previous literature were collected for model validation [59,60]. The quiet stance state of the foot was simulated by

applying a preload of 350 N to the plate under the foot model, while a tendon force of 75% of the 70 kg bodyweight was exerted on the calcaneus [5].

The model was further validated in dynamic gait loading by continuously simulating the support phases of a gait cycle based on the present model with a normal working speed of 1.2 m/s. The model boundary conditions for dynamic gait loading are shown in Fig. 2. The ground was simulated by a rigid plate and a total of six degrees of freedom were constrained. The initial angle between the foot and the ground was set to 18°. Simplified gait loading conditions were implemented on the model by imposing a rotation angle-time series and a simulated ground-support force-time series at the talus, which were obtained from normalized experimental data in the literature [62]. The static friction coefficient between the foot and the rigid plate was set to 0.6 according to the previous recommendation [63].

Then, the peak pressures of seven different plantar regions were extracted and compared with the literature [12,13,61]. The COP trajectory of the present gait simulation was also obtained and compared with the corridor extracted from experiments on 215 healthy volunteers in the literatures [14,15]. The COP trajectory was calculated using the following equation [9, 64]

$$\text{COP}(X, Y) = \left[\sum (\text{pressure} \times x - \text{coordinate}) / \sum \text{pressure}, \sum (\text{pressure} \times y - \text{coordinate}) / \sum \text{pressure} \right] \quad (2.1)$$

where the COP trajectory was calculated by summing the product of the pressures recorded by each ground element in the model with its (x and y) coordinates and then dividing it by the total pressure recorded by all ground elements.

2.3. Personalisation analysis of the foot-ankle model

Further, five healthy volunteers (172 cm and 60.4 kg on average) were recruited in gait experiments for the investigation of model personalisation methods. Their subject-specific models were established by coupling geometry scaling and material personalisation. Then, biomechanical responses of the subject-specific models based on MRI and optical scans were compared in dynamic gait loading conditions to explore their differences. Details about the personalisation process and comparative analysis were introduced.

Basic information about the five volunteers is listed in Appendix 1. All participants were required to provide a written informed consent to participate in this study. As presented in the previous study [65], MRI or CT scan for model reconstruction is anatomically accurate but time-consuming and expensive. Sometimes, it is impractical for use on a per-patient basis. For foot geometry scaling, optical scans are cheap, fast, and more practical for each patient. Here, the accuracy of the personalisation method with the optical scan was compared to that with the MRI scan. In addition, the shear wave elastography (SWE) method was adopted to define individual model parameters of plantar soft tissues corresponding to the volunteers.

First, all volunteers were asked to take an MRI scan of the foot-ankle anatomical structure and an optical scan of the foot-ankle geometric surface. The MRI scan was conducted in Xiangya hospital with a 3.0 T Magnetom Prisma MRI system (Siemens Ltd, Germany). The optical scan was performed using an EinScan 3D scanner (SHINING 3D, China). Then, a Tactilus® Foottrax (Sensor Products Inc. USA) pressure platform, with a sensor active area of 400 × 400 mm and 2704 individual sensors, was used for pressure measurement during a gait cycle. When passing the pressure plate, the volunteers were instructed not to look down but to look at a horizontal fixed point a certain distance away

[61]. Successful trials required that the volunteer's foot spontaneously contact the pressure plate at the second step. Each volunteer completed a total of eight successful gait trials on the right foot from the same starting position.

Developing a subject-specific model is a complex and time-consuming process. Thus, morphing an existing FE model into a personalised model is generally considered an efficient method to help describe the population variability. Kriging and radial basis function interpolation methods were commonly adopted in previous studies [28, 66–69] for model the geometry scale. The dual kriging algorithm was adopted for model scale referring to a previous study, which was proposed by Delorme et al. [70]. The kriging equations in 3D modelling were expressed as follows:

$$u(x) = a_0^x + a_1^x x + a_2^x y + a_3^x z \\ + \sum_{j=1}^n b_j^x \left(\sqrt{(x - x_j)^2 + (y - y_j)^2 + (z - z_j)^2} \right)$$

$$u(y) = a_0^y + a_1^y x + a_2^y y + a_3^y z \\ + \sum_{j=1}^n b_j^y \left(\sqrt{(x - x_j)^2 + (y - y_j)^2 + (z - z_j)^2} \right)$$

$$u(z) = a_0^z + a_1^z x + a_2^z y + a_3^z z \\ + \sum_{j=1}^n b_j^z \left(\sqrt{(x - x_j)^2 + (y - y_j)^2 + (z - z_j)^2} \right)$$

where $u(x, y, z)$ represent the node coordinates of the target finite element model and (x, y, z) represents the initial coordinates of the arbitrary model node. (x_j, y_j, z_j) represent the coordinates of the source feature point. n is the number of feature points and a_0, a_1, a_2, a_3, b_j are the coefficients that can be calculated using the following formulae:

$$\begin{bmatrix} 1X_1Y_1Z_1 \\ k(h)..... \\ 1X_nY_nZ_n \\ 1...10000 \\ X_1....X_n0000 \\ Y_1....Y_n0000 \\ Z_1....Z_n0000 \end{bmatrix} \times \begin{bmatrix} b_1^x b_1^y b_1^z \\ \\ b_n^x b_n^y b_n^z \\ a_0^x a_0^y a_0^z \\ a_1^x a_1^y a_1^z \\ a_2^x a_2^y a_2^z \\ a_3^x a_3^y a_3^z \end{bmatrix} = \begin{bmatrix} u_1^x u_1^y u_1^z \\ \\ u_n^x u_n^y u_n^z \\ 000 \\ 000 \\ 000 \\ 000 \end{bmatrix}$$

$$k(h) = \begin{bmatrix} k(0)...k(|X1 - Xn|) \\ \\ (|X1 - Xn|)...k(0) \end{bmatrix}$$

where (x_i, y_i, z_i) are the coordinates of the target feature points and (u_i^x, u_i^y, u_i^z) are the coordinates of the source feature points.

A series of source and associated target control points were selected to perform a kriging transformation for the foot-ankle model. A total of 47 skin surface landmarks were predefined for the model targeting the optical scans, and another 58 anatomical landmarks on bones were added for the foot-ankle model targeting the MRI scans. Accessible points on the skin, with evident bone protrusion structures and additional shape control points, were chosen as control points [25,71,72]. The control points on internal bone structures were primarily based on its anatomical features.

In addition, the material properties of plantar tissues in the model were subject-specific based on in vivo measurements using the SWE

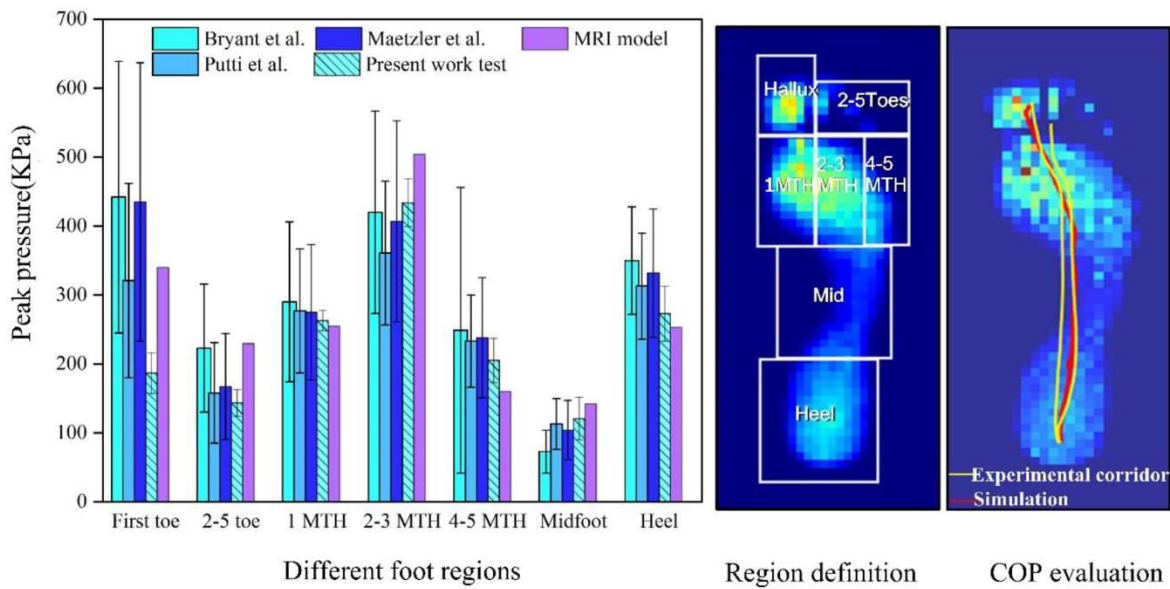


Fig 3. Evaluation of plantar pressure variation during the support phases of a gait cycle: regional peak plantar pressure, and COP trajectory. The foot was separated into seven regions to analyze plantar pressure difference. The plantar region pressure of the present model simulation results are represented by purple histogram, and the experimental data from the literature and the present study are represented by different blue histograms. The COP curve corridor obtained from the experimental data (represented by yellow) is introduced to compare with the simulation results of the present model (represented by red).

Table 3

Summary of regional peak plantar pressures of gait loading and its comparison with model simulation results

Reference	Bryant et al., 2000 [61]	Putti et al., 2007 [13]	Maetzler et al., 2010 [12]	Present experiment	Present model simulation
Instrument	EmedNovel, Germany 4sensor/cm ²	EmedNovel, Germany 4sensor/cm ²	EmedNovel, Germany 2 sensor/cm ²	Tactilus® Foottrax, USA 4 sensor/cm ²	Initial general model
Volunteer (Male/Female)	30(18/12)	53(17/36)	23(14/9)	5(5/0)	1(1/0)
Age	39.8(23-68)	34.4(19-52)	36(11.6)	24	23
Wight (kg)	70.1(48-96)	74.2(44-120)	66(10)	69(7.5)	69
BMI(kg/m ²)	-	-	24.5(3.95)	23.6(1.6)	23.1
First toe (kPa)	442(197)	321(141)	435(202)	196.6(29.6)	340
2-5 toe (kPa)	223(93)	158(73)	167(77)	143.4(19.5)	229.4
1 MTH (kPa)	290(116)	277(90)	275(98)	262.9(14.7)	255.0
2-3 MTH (kPa)	420(147)	361(104)	407(146)	434.0(34.8)	504.3
4-5 MTH (kPa)	249(207)	233(67)	238(87)	205.2(31.9)	160.0
Midfoot (kPa)	73(31)	113(37)	104(43)	120.6(31.0)	142.4
Heel (kPa)	350(78)	313(77)	332(93)	273.0(39.8)	252.9

Note: MTH represents metatarsal head.

method. Plantar tissue material properties of different foot regions of each volunteer were measured in five trials. The average values of shear modulus were adopted in the model, as presented in our previous study [34]. In this way, both personalised geometric and material characteristics were obtained simultaneously.

Five personalised foot-ankle models of the volunteers were established to compare the difference of the personalised methods with MRI and optical scans. The subject-specific models were obtained by morphing the above-mentioned original model based on kriging transformation and SWE measurements. Then, dynamic simulations of the support phases of a gait cycle with these models were implemented to analyse the difference between the two personalised model types. The biomechanical responses of the two personalised model types of five volunteers were compared by analysing plantar pressure and deep plantar soft tissue deformation. Plantar peak pressures and maximum deep soft tissue strains were statistically analysed in four stages during the gait simulation: foot strike, mid stance, terminal stance, and pre-swing stance.

3. Results

3.1. Evaluation of the deformation and kinematics of the foot-ankle FE model

The regional peak pressure and COP verification results in dynamic gait loading are shown in Fig. 3 and Table 3. As seen from the peak pressure results in different foot regions during the support phases of a gait cycle, the peak pressures predicted by the model and measured in the current experiments are all in the range presented in the previous studies [12,13,61]. However, the peak pressures predicted by the present model are out of the experimental ranges for the big toe and mid forefoot regions. Here, the experimental design is aimed at analysing the following personalisation investigation, and thus it only included five volunteers. This model is still a general model based on previously scanned human data. This also indicated that model personalisation was necessary for subject-specific pressure analysis, and individual variability significantly influenced the plantar pressure values. As shown in Fig. 3, the COP curve in the red line predicted by the present model also

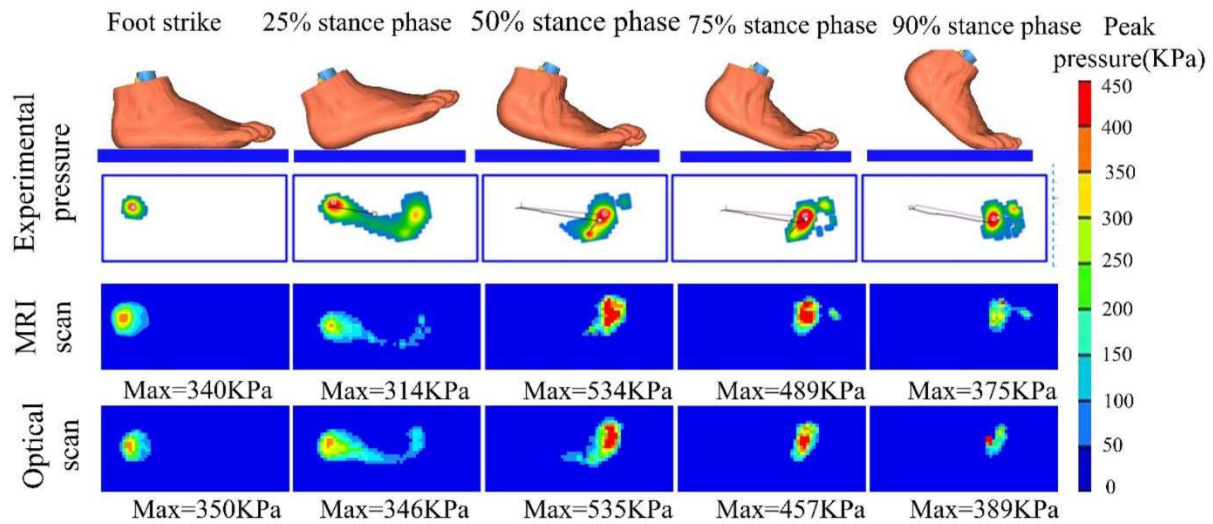


Fig 4. Comparison of plantar pressures during the support phases of a gait cycle (subject 1)

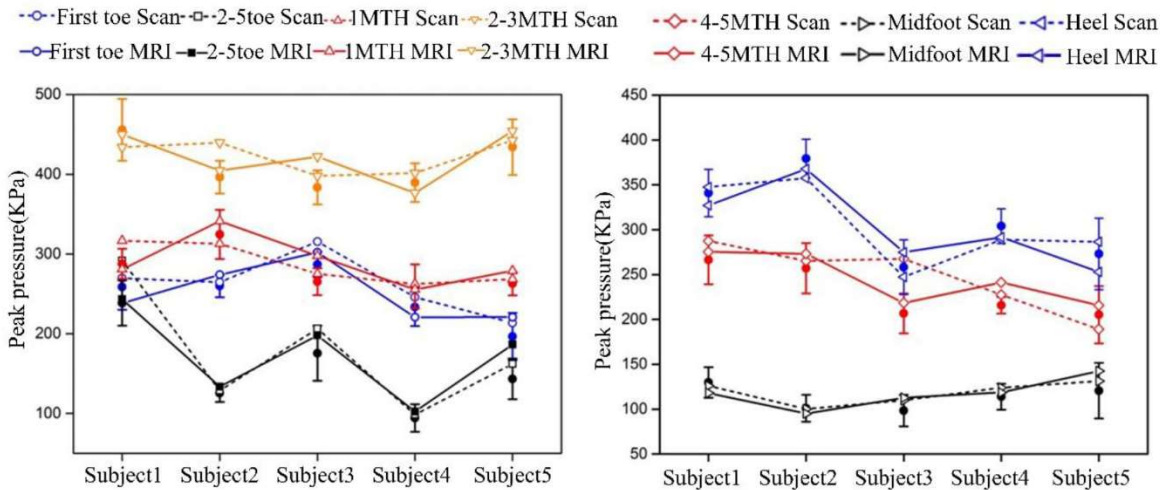


Fig 5. Comparison of plantar peak pressures of different models and experimental results. The abscissa lists the five volunteers. All solid lines represent the simulation results of the MRI-based models, whereas dotted lines represent the simulation results of the optical-based models. The cylindrical deviation with an average describes the experimental corridor. The pressure information in different plantar regions is distinguished by different line colors.

correlated well with the corridor proposed by Cock et al. [73].

3.2. Comparative analysis of two personalised foot-ankle model types

Plantar pressure distributions of a typical subject-specific experiment and two model simulation results during the support phases of a gait cycle are illustrated in Fig. 4. The two personalised model types are based on MRI scan and optical scan, respectively. The two models also included material personalisation concerning the individual elastic modulus variability of plantar tissues. The subject-specific shear moduli measured by the SWE method are listed in Table 1 of the Appendix. Notably, both the regions and values of peak plantar pressures in different gait phases are in good agreement, regardless of the experiment and simulation models, although the simulation results with the two models always present slight differences.

The comparison of regional plantar peak pressures of the subject-specific experimental results and the simulation results of the two model types are shown in Fig. 5. Experimental data corridors of different gait phases of five volunteers are established using eight gait cycle trials per volunteer, which are shown by columnar deviations. The solid lines represent the simulation results from the MRI-based model, whereas the

dashed lines represent the simulation results from the optical-based model. Different colours represent different plantar regions. Most simulation results from both models were in the experimental corridors. The deviation of the simulation results from the experimental mean value varied from 0.2% to 14.2% for the MRI-based model, and from 0.5% to 17.5% for the optical-based model. This also indicates the robustness of our personalisation methods with both geometric scan data and SWE measurements.

Then, the Mann Whitney U test was adopted to analyse the difference in the simulation results of the optical-based and MRI-based models from the experimental gait data. Both statistical hypotheses indicate no difference between the plantar peak pressures of these two model simulation results and the experimental gait data. Considering all volunteer data in different phases, the *p* values of MRI-based and optical-based model simulation results with respect to the gait experimental average values were 0.71 and 0.46, respectively (*p* > 0.05). Therefore, the statistical hypothesis is retained. This means that there is no significant difference between the gait experimental data and the simulation results of both personalised model types in plantar peak pressure response. No significant difference was assumed between the simulation results of both personalised methods. The obtained *p* value was 0.86 (>

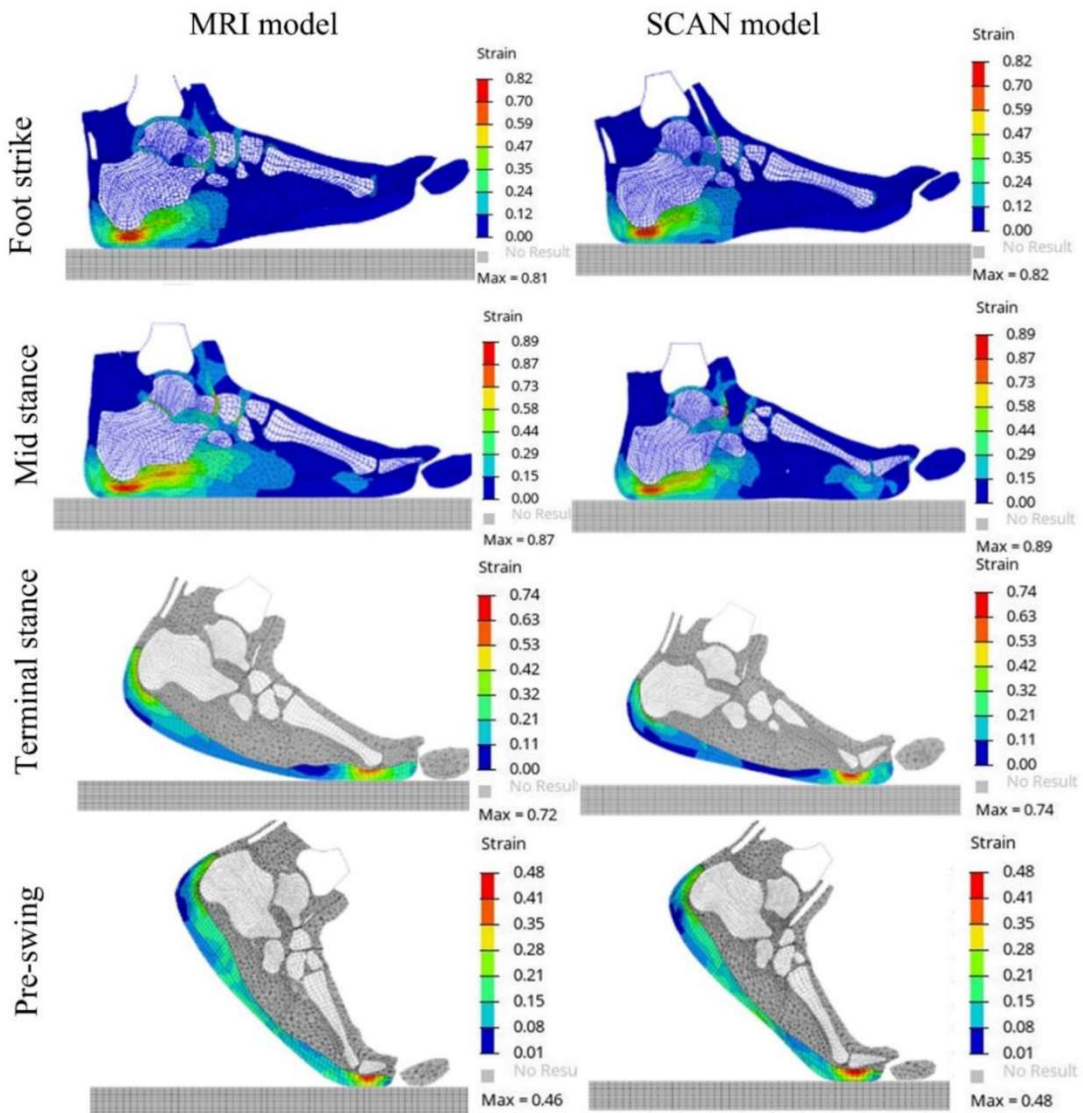


Fig 6. Comparison of plantar tissue strain during the support phases of a gait cycle (subject 1).

0.05), which indicated that no significant difference existed in exploring plantar peak pressure using both model types.

Further, the strain responses of the internal soft tissues of the two personalised model types during the support phases of a gait cycle were compared to verify the model consistency. A typical animation comparison of subject 2 is shown in Fig. 6. The foot regions with the largest strains were identical for the two model types in different gait phases.

The comparison of peak strain values of both personalised model types for the five volunteers during the support phases of a gait cycle is shown in Fig. 7. The solid lines represent the simulation results from the MRI-based model, whereas the dashed lines represent the simulation results from the optical-based model. Different colours represent different gait phases. Evidential differences of predicted peak strains can be noted for both model types in the foot strike and pre-swing phases. The largest deviation of the optical-based model from the MRI-based model reached 14.8% and several large deviations existed in subjects 2, 3, and 5. With the same statistical method in peak pressure analysis, the obtained p value of the Mann Whitney U test, considering the strain results of both model types, was 0.904 (> 0.05). Therefore, the original hypothesis that no significant difference existed in predicting plantar deformation of deep soft tissues between both personalisation methods was retained.

4. Discussion

The biggest advantage of a three-dimensional finite element model is the exploration of biomechanical responses of complex foot-ankle structures, especially concerning in-deep tissue deformation, at low costs. Furthermore, the influence of model variables and the investigation of non-accessible loading conditions can easily be incorporated. This is undoubtedly a prerequisite for further strengthening the treatment of diabetic foot ulcers, joint degeneration, ligament injury, or other medical treatment programs and designing appropriate foot orthoses. This study established a detailed foot-ankle finite element model with updated main soft tissues based on our first version and validated it in both static standing and dynamic gait loading conditions. Most previous foot-ankle finite models were validated with experiments concerning specific applications and generally used quasi-static gait phases at a specific time to represent realistic dynamic gait. Here, the model was validated in dynamic gait loading conditions by comparing simulation results with a review of previous and new gait experimental data. Both regional plantar peak pressures and COP curves were in good agreement with the experimental data. As experimental sensor density can influence peak pressure, the model mesh also presented potential influences on simulated peak pressure values. Thus, a corresponding mesh density

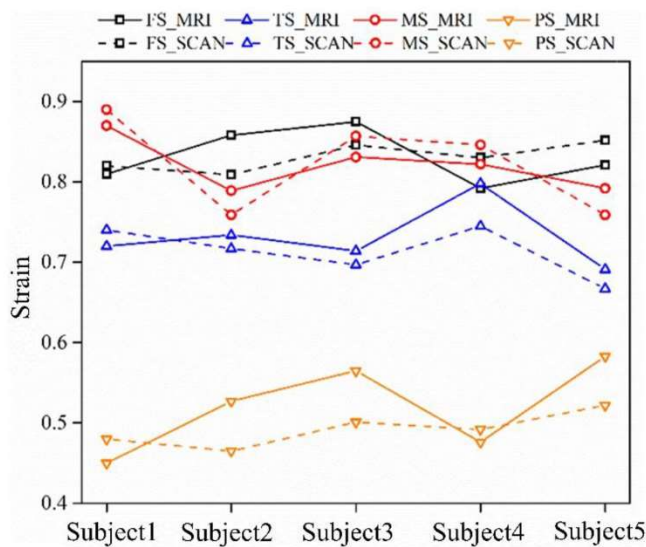


Fig 7. Comparison of plantar tissue strain of different models during the support phases of a gait cycle (Foot Strike (FS), Mid Stance (MS), Terminal Stance (TS), and Pre-swing Stance (PS)). The abscissa lists the five volunteers, and the ordinate is the maximum strain values of plantar soft tissue in different gait phases. All solid lines represent the simulation results of the MRI-based models, whereas the dotted lines represent the simulation results of the optical-based models. The strain information in different gait phases is distinguished by different line colors.

of the experimental device should be selected for proper validation. In summary, the global validation from static standing loading to dynamic gait loading and from surface pressure to structure deformation proved the robustness of the present model.

When comparing gait simulation results of optical scan and MRI scan models, both peak plantar pressure and deep tissue von mises strain presented a non-significant difference during the support phase of an entire gait cycle. However, a large deviation of strain values was observed when the heel hit the ground. This should be attributed to different model personalised processes. The MRI-based model included more accurate personalised bone structures based on bone controlling points, whereas the bone structure of the optical-based model was scaled only by skin controlling points. In conclusion, the optical scan is sufficient for FE model scaling based on the simulation results of plantar pressure and soft tissue deformation.

In addition, most previous studies [21,74,75] personalised finite element models only considering subject-specific geometry or anatomy structure. The difference between human bodies is largely related to its tissue properties. As indicated by our previous study, mechanical responses of the foot-ankle model in static loading were largely affected by its material properties. Other studies also indicated that in the development of parametric FE human body models, the changes of geometry, composition, and material properties would lead to significantly different biomechanical responses [66,76,77]. Thus, the present study also considered material personalisation using SWE measurements. In the future, this method can be further extended for other biomechanical models because material property change can be dominant, especially concerning pathology-related research such as diabetic foot and heel pain. Here, the SWE method can only *in vivo* measure the variation of the elastic modulus. Other methods need to be developed in the future to further improve the accuracy of model material personalisation.

The present study also has its limitations. A simplified gait loading condition was implemented on the foot-ankle model to achieve a realistic gait analysis. Although the effects of muscle forces were partly included by imposing the ground-support force-time series, this method cannot fully reflect the tension effects of the muscle forces on detailed foot structures such as some ligament or joint deformations. However,

this method is efficient in terms of computational cost, and sufficient for the following comparative analysis focussed on plantar tissue deformation. Detailed muscle effects on foot biomechanical behaviours can be further investigated in the future by coupling the musculoskeletal and FE models. In addition, the scaled model created using the kriging interpolation algorithm can have differences at the joints compared with the original model. The present study primarily focused on analysing plantar pressure and plantar tissue deformation, whereas joint forces were not investigated. In the future, especially concerning the model's application to the foot-ankle joint analysis, further validation and analysis related to joint stress or pressure is needed.

5. Conclusion

In this study, a three-dimensional finite element foot-ankle model was established with detailed soft tissue definitions and validated in both, static stance and dynamic gait loading environments. The model simulation results in dynamic gait loading were compared with a review of a series of gait experimental data. Both regional plantar pressures and COP curves predicted by the model correlated well with the corridors recorded in the experimental tests. This demonstrates the current model's availability and robustness in gait analysis. Thus, it can be further used for related pathology analysis or treatment design for diabetic and flatfoot patients.

Then, to provide a model basis for designing custom devices, model personalisation methods were investigated based on MRI scan and optical scan by analysing subject-specific foot-ankle mechanical behaviours in dynamic gait loading with both experimental and simulation results. Subject-specific material definition of plantar soft tissues were also adopted in model personalisation through *in vivo* SWE measurements. The comparative analysis showed that both personalisation methods show a good agreement with the experimental results regarding plantar pressure distribution and plantar soft tissue deformation. Non-significant differences were noted for these indexes in the supporting stages of a gait cycle. Thus, the present model with a fast optical scan personalisation method of specific SWE measurement should be sufficient, rather than a complex MRI scan scaling method, for subject-specific plantar deformation behaviour analysis during dynamic gait loading for an efficient clinical application.

CRediT authorship contribution statement

Fuhao Mo: Conceptualization, Writing – original draft, Project administration, Funding acquisition. **Yuandong Li:** Methodology, Validation, Investigation, Formal analysis. **Junjie Li:** Investigation, Software. **Shuangyuan Zhou:** Resources, Data curation, Writing – review & editing. **Zurong Yang:** Writing – review & editing, Visualization.

Declaration of Competing Interest

The authors declare that they have no known competing financial interests or personal relationships that could have appeared to influence the work reported in this paper.

Acknowledgments

This work is supported by the National Natural Science Foundation of China (Grant No. 51875187), National Key R&D Program of China (2017YFF0206602), Hunan Youth Talent Program (Grant No. 2020RC3016), and Key Research and Development Program of Hunan Province of China (Grant No. 2022SK2105).

Appendix

Table A1

Table A1

Subject information and individual shear modulus measured by SWE method

	Subject1	Subject2	Subject3	Subject4	Subject5
Height(cm)	175	167	177	170	173
Weight(kg)	58	52	70	57	65
BMI	18.9	18.6	22.3	19.7	21.7
Stiffness (kPa)					
Micro-chamber	20(2.2)	18.9 (4.6)	22.4 (4.3)	26.7 (3.9)	24.9 (2.4)
Macro-chamber	11.5(1.8)	11.4 (2.8)	10.8 (3.2)	11.3 (1.2)	12.2 (2.8)
Whole heel pad	15.9(1.5)	12.6 (1.2)	15.7 (1.4)	14.0 (1.6)	15.5 (2.5)
Big-toe	16.2(4.7)	11.7 (1.8)	15.0 (1.2)	13.5 (0.9)	14.2 (1.9)
First metatarsal	12.1 (1.43)	8.2(0.9)	12.1 (1.1)	11.7 (2.4)	10.6 (1.2)
Fourth metatarsal	13.6(2.5)	10.1 (2.4)	13.5 (1.1)	16.6 (2.2)	14.1 (2.1)

References

- [1] Chen TL, Wong DW, Wang Y, Lin J, Z M. Foot arch deformation and plantar fascia loading during running with rearfoot strike and forefoot strike: a dynamic finite element analysis. *J Biomech* 2018;83:260–72.
- [2] Isvilanonda V, Dengler E, Iaquinto JM, Sangeorzan BJ, Ledoux WR. Finite element analysis of the foot: Model validation and comparison between two common treatments of the clawed hallux deformity. *Clin Biomech* 2012;27(8):837–44.
- [3] Ahanchian N, Nester CJ, Howard D, Renc L, Parker D. Estimating the material properties of heel pad sub-layers using inverse Finite Element Analysis. *Med Eng Phys* 2016;40:11–9.
- [4] Chen W, Lee T, Lee PV, Lee JW, Lee S. Effects of internal stress concentrations in plantar soft-tissue-A preliminary three-dimensional finite element analysis. *Med Eng Phys* 2010;32(4):324–31.
- [5] Cheung T, Zhang M, An K. Effect of Achilles tendon loading on plantar fascia tension in the standing foot. *Clin Biomech* 2006;21(2):194–203.
- [6] Shin J, Yue N, Untaroiu CD. A finite element model of the foot and ankle for automotive impact applications. *ann biomed eng* 2012;40(12):2519–31.
- [7] Tao K, Wang D, Wang C, Wang X, Liu A, Nester CJ, Howard D. An In Vivo experimental validation of a computational model of human foot. *J Bionic Eng* 2009;6(4):387–97.
- [8] Cheung JT, Zhang M, Leung AK, F Y. Three-dimensional finite element analysis of the foot during standing — a material sensitivity study. *J Biomech* 2004;38(5): 1045–54.
- [9] Wong WC, Niu W, Wang Y, Zhang M, Ren L. Finite element analysis of foot and ankle impact injury: risk evaluation of calcaneus and talus fracture. *PLoS One* 2016;11(4). e0154435-e0154435.
- [10] Actis RL, Ventura LB, Lott DJ, Smith KE, Commeen PK, Hastings MK, Mueller MJ. Multi-plug insole design to reduce peak plantar pressure on the diabetic foot during walking. *Med Biol Eng Comput* 2008;46(4):363–71.
- [11] Bus SA, Ulbrecht JS, Cavanagh PR. Pressure relief and load redistribution by custom-made insoles in diabetic patients with neuropathy and foot deformity. *Clin Biomech* 2004;19(6):629–38.
- [12] Maetzler M, Bochdansky T, Abboud RJ. Normal pressure values and repeatability of the Emed® ST2 system. *Gait Posture* 2010;32(3):391–4.
- [13] Putti AB, Arnold GP, Cochrane L, Abboud RJ. The Pedar in-shoe system: repeatability and normal pressure values. *Gait Posture* 2007;25(3):401–5.
- [14] Buldt AK, Forghany S, Landorf KB, Murley GS, Levinger P, Menz HB. Centre of pressure characteristics in normal, planus and cavus feet. *J Foot Ankle Res* 2018;11(1):1–9.
- [15] Chiu MC, Wu HC, Chang LY. Gait speed and gender effects on center of pressure progression during normal walking. *Gait Posture* 2013;37(1):43–8.
- [16] Mo F, Zheng Z, Zhang H, Li G, Yang Z, Sun D. In vitro compressive properties of skeletal muscles and inverse finite element analysis: Comparison of human versus animals. *J Biomech* 2020;109.
- [17] Chen Y, Chang C, Li C, Chang C, Lin C. Finite element analysis of plantar fascia during walking: a quasi-static simulation. *Foot Ankle Int* 2015;36(1):90–7.
- [18] Tarrade T, Dakhil N, Behr M, Salin D, Llari M. Real-time analysis of the dynamic foot function: a machine learning and finite element approach. *J Biomech Eng* 2021;143(4).
- [19] Akrami M, Qian Z, Zou Z, Howard D, Nester CJ, Ren L. Subject-specific finite element modelling of the human foot complex during walking: sensitivity analysis of material properties, boundary and loading conditions. *Biomech Model Mechanobiol* 2018;17(2):559–76.
- [20] Guiotto A, Sawacha Z, Guarneri G, Avogaro A, Cobelli C. 3D finite element model of the diabetic neuropathic foot: a gait analysis driven approach. *J Biomech* 2014; 47(12):3064–71.
- [21] Bucki M, Luboz V, Perrier A, Champion E, Diot B, Vuillerme N, Payan Y. Clinical workflow for personalized foot pressure ulcer prevention. *Med Eng Phys* 2016;38 (9):845–53.
- [22] Ni M, Niu W, Wong WC, Zeng W, Mei J, Zhang M. Finite element analysis of locking plate and two types of intramedullary nails for treating mid-shaft clavicle fractures. *Injury* 2016;47(8):1618–23.
- [23] Gefen A. Plantar soft tissue loading under the medial metatarsals in the standing diabetic foot. *Med Eng Phys* 2003;25(6):491–9.
- [24] Bucki M, Luboz V, Perrier A, Champion E, Diot B, Vuillerme N, Payan Y. Clinical workflow for personalized foot pressure ulcer prevention. *Med Eng Phys* 2016;38 (9):845–53.
- [25] Lochner SJ, Huissoon JP, Bedi SS. Development of a patient-specific anatomical foot model from structured light scan data. *Comput Meth Biomed Eng* 2014;17:9–12.
- [26] Zhang C, Ji X. Statistical ankle-shape and pressure analysis for design of elastic tubular bandage. In: Proceedings of the Institution of Mechanical Engineers Part H Journal of Engineering in Medicine. 235; 2020.
- [27] Stankovi K, Huysmans T. D. F, Subject-specific identification of three dimensional foot shape deviations using statistical shape analysis. *Expert Syst Appl* 2020;151: 113372.
- [28] Grant T M, Diamond L E, Pizzolato C, et al. Development and validation of statistical shape models of the primary functional bone segments of the foot. *PeerJ* 2020;8(8). e8397.
- [29] Carbone V, Fluit R, Pellikaan P. TLEM 2.0 – A comprehensive musculoskeletal geometry dataset for subject-specific modeling of lower extremity. *J Biomech* 2015;48(5):734–41.
- [30] Shim V B, Fernandez J W, Gamage P B. Subject-specific finite element analysis to characterize the influence of geometry and material properties in Achilles tendon rupture. *J Biomech* 2014;47(15).
- [31] Buschmann WR, Jahss MH, Kummer F, Desai P, Gee RO, Ricci JL. Histology and histomorphometric analysis of the normal and atrophic heel fat pad. *Foot Ankle Int* 1995;16(5):254–8.
- [32] Jahss MH, Michelson JD, Desai P, Kaye R, Kummer F, Buschman W, Watkins F, Reich S. Investigations into the fat pads of the sole of the foot: anatomy and histology. *Foot Ankle* 1992;13(5):233–42.
- [33] Tsai WC, Wang CL, Hsu TC, Hsieh FJ, Tang FT. The mechanical properties of the heel pad in unilateral plantar heel pain syndrome. *Foot Ankle Int* 1999;20(10): 663–8.
- [34] Mo F, Li J, Yang Z, Zhou S, Behr M. In Vivo measurement of plantar tissue characteristics and its indication for foot modeling. *Ann Biomed Eng* 2019;47(2): 2356–71.
- [35] Carter D, H W. Bone compressive strength: the influence of density and strain rate. *Science* 1976;194(4270):1174–6.
- [36] Mo F, Arnoux PJ, Cesari D, Masson C. The failure modelling of knee ligaments in the finite element model. *Int J Crashworthiness* 2012;17(6):630–6.
- [37] Mo F, Li F, Behr M, Xiao Z, Zhang G, Du X. A lower limb-pelvis finite element model with 3D active muscles. *Ann Biomed Eng* 2018;46(1):86–96.
- [38] Nie B, Panzer MB, Mane A, Mait AR, Donlon J, Forman JL, K RW. Determination of the in situ mechanical behavior of ankle ligaments. *J Mech Behav Biomed Mater* 2017;65:502–12.
- [39] Nie B, Forman JL, Panzer MB, Mait AR, Donlon JP, Kent R. Fiber-based modeling of in situ ankle ligaments with consideration of progressive failure. *J Biomech* 2017; 61:102–10.
- [40] Mo F, Li J, Dan M, Liu T, Behr M. Implementation of controlling strategy in a biomechanical lower limb model with active muscles for coupling multibody dynamics and finite element analysis. *J Biomech* 2019;92:51–60.
- [41] Al-Dirini RM, Reed MP, Hu J, Thewlis D. Development and validation of a high anatomical fidelity FE model for the buttock and thigh of a seated individual. *Ann Biomed Eng* 2016;44(9):1–12.
- [42] Crowninshield RD, Nakanura S. An analysis of soft tissue loading in the foot. *J Biomech* 1981;14(7):492–492.
- [43] Dakin GJ, Arbelaez RA, Molz FT, Alonso JE, Mann KA, Eberhardt AW. Elastic and viscoelastic properties of the human pubic symphysis joint: effects of lateral impact joint loading. *J Biomech Eng* 2001;123(3):218–26.
- [44] Funk JR, Hall GW, Crandall JR, Pilkey WD. Linear and quasi-linear viscoelastic characterization of ankle ligaments. *J Biomech Eng* 2000;122(1):15.
- [45] Davis WH, Sobel M, DiCarlo EF, Torzilli PA, Deng X, Geppert MJ, Patel MB, Deland J. Gross, histological, and microvascular anatomy and biomechanical testing of the spring ligament complex. *Foot Ankle Int* 1996;17(2):95–102.
- [46] Kura H, Luo ZP, Kitaoka HB, Smutz WP, An K. Mechanical behavior of the lisfranc and dorsal cuneometatarsal ligaments: in vitro biomechanical study. *J Orthop Trauma* 2001;15(2):107–10.
- [47] Kitaoka HB, Luo ZP, Grawny ES, Berglund LJ, An K. Material properties of the plantar aponeurosis. *Foot Ankle Int* 1994;15(10):557–60.
- [48] Isvilanonda, V., Finite element modeling of the foot, 2015.
- [49] Morrison SM, Dick TJ, M J. Structural and mechanical properties of the human Achilles tendon: sex and strength effects. *J Biomech* 2015;48(12):3530–3.
- [50] Maganaris CN, Paul JP. In vivo human tendon mechanical properties. *J Physiol* 1999;521(1):307–13.
- [51] Magnusson SP, Narici MV, Maganaris CN, Kjaer M. Human tendon behaviour and adaptation, in vivo. *J Physiol* 2008;586(1):71–81.
- [52] Zajac FE. Muscle and tendon: Properties, models, scaling, and application to biomechanics and motor control. *Crit Rev Biomed Eng* 1989;17(4):359–411.
- [53] Erdemir A, Viveiros ML, Ulbrecht JS, Cavanagh PR. An inverse finite-element model of heel-pad indentation. *J Biomech* 2006;39(7):1279–86.
- [54] Chen WM, Lee VS. Explicit finite element modelling of heel pad mechanics in running: inclusion of body dynamics and application of physiological impact loads. *Comput Meth Biomed Eng* 2014;18(14):1582–95.

- [55] Hsu C, Tsai W, Hsiao T, Tseng F, Shau Y, Wang C, Lin S. Diabetic effects on microchambers and macrochambers tissue properties in human heel pads. *Clin Biomech* 2009;24(8):682–6.
- [56] Bandholm T, Boysen L, Haugaard S, Zebis MK, Bencke J. Foot medial longitudinal-arch deformation during quiet standing and gait in subjects with medial tibial stress syndrome. *J Foot Ankle Surg* 2008;47(2):89–95.
- [57] Cavanagh PR, Morag EE, Boulton AJM, Young MJ, Deffner KT, Pammer SE. The relationship of static foot structure to dynamic foot function. *J Biomech* 1997;30(3):243–50.
- [58] Williams DS, McClay IS. Measurements used to characterize the foot and the medial longitudinal arch: reliability and validity. *Phys Ther* 2000;80(9):864–71.
- [59] Birtane M, Tuna H. The evaluation of plantar pressure distribution in obese and non-obese adults. *Clin Biomech* 2004;19(10):1055–9.
- [60] Cavanagh PR, Rodgers MM, Libosha A. Pressure distribution under symptom-free feet during barefoot standing. *Foot Ankle* 1987;7(5):262–78.
- [61] Bryant A, Tinley P, Singer K. Normal values of plantar pressure measurements determined using the EMED-SF system. *J Am Podiatr Med Assoc* 2000;90(6):295.
- [62] Aubin PM, Whittaker E, Ledoux WR. A robotic cadaveric gait simulator with fuzzy logic vertical ground reaction force control. *IEEE Trans Rob* 2012;28(1):246–55.
- [63] Zhang M, Mak A. In vivo friction properties of human skin. *Prosthetics Orthotic Int* 1999;23(2):135–41.
- [64] Zhang H, Zanotto D, Agrawal S. Estimating CoP trajectories and kinematic gait parameters in walking and running using instrumented insoles. *IEEE Robotic Automat Lett* 2017;4(2):2159–65.
- [65] Lochner SJ, Huissoon JP, Bedi SS. Development of a patient-specific anatomical foot model from structured light scan data. *Comput Meth Biomech Biomed Eng* 2014;11(7):1198–205.
- [66] Zhang K, Cao L, Fanta A, Reed MP, Neal M, Wang J, Lin C, Hu J. An automated method to morph finite element whole-body human models with a wide range of stature and body shape for both men and women. *J Biomech* 2017;60:253–60.
- [67] Beillas P, Berthet F. An investigation of human body model morphing for the assessment of abdomen responses to impact against a population of test subjects. *Traffic Inj Prev* 2017;18(1):142–7.
- [68] Lalonde NM, Petit Y, Aubin C, Wagnac E, Arnoux P. Method to geometrically personalize a detailed finite-element model of the spine. *IEEE Trans Biomed Eng* 2013;60(7):2014–21.
- [69] Liu S, Beillas P, Li D, Wang X. Morphing an Existing Open Source Human Body Model into a Personalized Model for Seating Discomfort Investigation. In: SAE International Conference Paper; 2020. p. 1–7.
- [70] Delorme S, Petit Y, de Guise JA, Labelle H, Aubin CE, Dansereau J. Assessment of the 3-d reconstruction and high-resolution geometrical modeling of the human skeletal trunk from 2-d radiographic images. *IEEE Trans Biomed Eng* 2003;50(8):989–98.
- [71] Stebbins J, Harrington M, Thompson N, Zavatsky A, Theologis T. Repeatability of a model for measuring multi-segment foot kinematics in children. *Gait Posture* 2006;23(4):401–10.
- [72] Witana CP, Xiong S, Zhao J, G RS. Foot measurements from three-dimensional scans: a comparison and evaluation of different methods. *Int J Ind Ergon* 2006;36(9):789–807.
- [73] Cock AD, Vanrenterghem J, Willems T, Witvrouw E. The trajectory of the centre of pressure during barefoot running as a potential measure for foot function. *Gait Posture* 2008;27(4):669–75.
- [74] Campanelli V, Fantini M, Faccioli N, Cangemi A, Pozzo A, Sbarbat A. Three-dimensional morphology of heel fat pad: an in vivo computed tomography study. *J Anat* 2011;219(5):622–31.
- [75] Luboz V, Perrier A, Bucki M, Diot B, Cannard F, Vuillerme N, Payan Y. Influence of the calcaneus shape on the risk of posterior heel ulcer using 3d patient-specific biomechanical modeling. *Ann Biomed Eng* 2015;43(2):325–35.
- [76] Hu J, Zhang K, Reed MP, Wang JT, Neal M, Lin CH. Frontal crash simulations using parametric human models representing a diverse population. *Traffic Inj Prev* 2019;20(1):97–105.
- [77] Wang Y, Cao L, Bai Z, Reed M, Rupp JD, Hoff CN, Hu J. A parametric ribcage geometry model accounting for variations among the adult population. *J Biomech* 2016;49(13):2791–8.